Clays Clay Miner., Vol. 70, No. 4:555–565, 2022
https://doi.org/10.1007/s42860-022-00201-9

ORIGINAL PAPER

Effect of temperature on the synthesis of g-C_3N_4/montmorillonite and its visible-light photocatalytic properties

Yao Li · Hongjuan Sun · Tongjiang Peng · Xiao Qing

Accepted: 24 August 2022 / Published online: 25 October 2022

Abstract Graphite phase carbon nitride (g-C_3N_4) is a non-metal semiconductor material with a suitable band gap (2.7 eV) for visible photocatalysis. However, the high cost of relevant synthesis methods and poor adsorption performance have limited its practical applications. The objective of the present study was to mitigate these problems by synthesizing the g-C_3N_4 in the presence of exfoliated montmorillonite (Mnt). Compared with bulk montmorillonite, the specific surface area of exfoliated two-dimensional Mnt layers was significantly increased. As a result, the light transmittance of the lamella improved noticeably due to the fact that a freshly exposed surface had a large number of active reaction sites, making Mnt an excellent carrier for the photocatalyst g-C_3N_4. In order to improve the photocatalytic performance of g-C_3N_4, a series of g-C_3N_4/Mnt composites was prepared by a wet chemical method using Mnt nanolayers as the matrix. X-ray diffraction, infrared spectroscopy, Brunauer-Emmett-Teller nitrogen adsorption/desorption, transmission electron microscopy, and ultraviolet-visible diffuse reflectance spectroscopy were used to analyze the phase structure, the chemical bonds, the specific surface area and pore sizes, the morphology, and the light absorption characteristics of the composites, respectively. Rhodamine B (RhB) served as the target dye to test the photocatalytic degradation performance of the composites under visible light. According to the findings, the surface of the Mnt nanolayers was densely and uniformly covered by g-C_3N_4, forming a multilayered stack structure. An increase of the calcination temperature improved the crystallinity of g-C_3N_4, leading first to densification and then to relaxation of the layered composite structure. Conversely, the band gap of the composite gradually decreased from 2.56 to 2.4 eV. Furthermore, temperature exposure changed the photocatalytic performance of the composite drastically. While the largest photocatalytic activity was observed at 610°C, it started to decrease with further heating of the composite. The complete degradation of RhB solution occurred after 2 h of visible light irradiation. The findings of the current study provide a scientific basis for the synthesis of a new generation of photocatalysts.

Keywords Calcination temperature · g-C_3N_4 · Montmorillonite · Nanolayers · Visible light catalysis

Associate Editor: Yael Mishael

Y. Li · H. Sun (✉) · T. Peng · X. Qing
Key Laboratory of Solid Waste Treatment and Resource Recycle, Southwest University of Science and Technology, Mianyang 621010, China
e-mail: sunhongjuan@swust.edu.cn

Introduction

Photocatalysis is of great importance in the fields of energy and environmental applications, and is regarded as a revolutionary technology in the 21st Century. Most photocatalysts (such as TiO_2 and GaN) exhibit wide band gaps within the range 2.0–3.4 eV (Fujishima et al., 2008). This enables their photocatalytic activity under ultraviolet light (<385 nm) to be enhanced, which, meanwhile, accounts for only 3% of the solar energy (Herron et al., 2015). In that regard, searching for a

highly active photocatalyst with visible light response and its practical application has attracted the attention of many scholars(Dong et al., 2014; Fatimah et al., 2011; Thomas et al., 2008).

Graphite phase carbon nitride (g-C_3N_4) is a non-metal semiconductor photocatalytic composite with a band gap (2.7 eV) suitable for the initiation of catalytic reactions under visible light. Moreover, g-C_3N_4 is an ecofriendly, non-toxic, non-polluting material that possesses stable physical and chemical properties, thus offering promise for a wide range of photocatalytic applications (Dong et al., 2014; Kumar et al., 2018; Wang et al., 2009).

Methods of synthesis of g-C_3N_4 include physical vapor deposition (PVD), high-temperature chemical vapor deposition (CVD), and hot melt techniques (Thomas et al., 2008; Li, Y.P., et al., 2014). However, all of them are costly and require stringent reaction conditions. In addition, unmodified g-C_3N_4 has no adsorption properties, and is easy to agglomerate, resulting in small specific surface area, high electron-hole recombination rate, and poor light utilization efficiency. These shortcomings reduce the photocatalytic efficiency of g-C_3N_4, thereby limiting its practical application (Xue et al., 2015).

Recently, research has been focused on supporting the multi-layered silicate mineral matrix to solve the problem of easy agglomeration and small specific surface area of photocatalysts and to extend their potential application range (Cheng et al., 2011; Fatimah et al., 2011; Peng et al., 2016). Increasing attention has been paid to montmorillonite as a promising carrier for photocatalysts due to its large specific surface area and good adsorption performance (Li, C. et al., 2016, 2018; Li et al., 2017; Sonawane et al., 2010; Sun et al., 2002). Also, attempts have been made to combine Mnt with graphite phase carbon nitride and to obtain materials with increased photocatalytic properties. For example, Li, S. et al. (2016) prepared a g-C_3N_4/Mnt composite with a g-C_3N_4 mass fraction of 31.8%, whose photocatalytic degradation rate in relation to RhB was four times greater than that of pure g-C_3N_4. Furthermore, combining g-C_3N_4 with Mnt as a carrier allowed those authors to solve the problem of g-C_3N_4 agglomeration effectively. According to Li et al. (2017), the g-C_3N_4/Mnt composite possessed a large specific surface area, good temperature resistance, and easy recycling, which help to improve its photo absorption characteristics. Moreover, the photocatalytic activity of the g-C_3N_4/Mnt composite prepared exceeded that of pure g-C_3N_4.

When water molecules get into the interlayer space of the Mnt 2:1 layers through an aqueous solution, the distance between the Mnt lamellae enlarges because of increasing interlayer penetration depth and peeling away of hydration layers. In this respect, compared with bulk montmorillonite, the specific surface area of exfoliated two-dimensional Mnt layers is increased significantly. This improves noticeably the light transmittance of the lamellae due to the fact that a freshly exposed surface has a large number of active reaction sites.

Given the above information, Mnt has the prospect of being a good photocatalytic support. However, some aspects still need to be clarified. Among these are the need to confirm an increase in specific surface area of exfoliated Mnt as the support for the g-C_3N_4 photocatalyst, and to study the photocatalytic effect of g-C_3N_4 in the g-C_3N_4/Mnt composite and its related mechanism. The objective of the present study was, therefore, to find answers to these questions by measuring the effect of temperature on the photocatalytic performance of a series of g-C_3N_4/Mnt composites, prepared by a wet chemical method using exfoliated Mnt as the matrix.

Experimental

Raw Materials and Reagents

The Mnt was prepared and exfoliated as follows. Bentonite (Santai City, Sichuan Province, China) was ground as a dry powder and passed through a 200-mesh sieve (74 μm), 10 g of which was combined with 0.6 g of anhydrous sodium carbonate in a 500 mL beaker, mixed by stirring, and then 160 mL of deionized water (with a resistivity of 18.2 MΩ • cm) was added, giving a a solid-liquid ratio of 1:10. The mixture was then stirred for 30 min in a water bath at 80°C to effect dispersion and sodium saturation. After that, the solid:liquid ratio was adjusted to 1:20 using deionized water, and the suspension was stirred in a high-speed homogenizer at a rotational speed of 10,000 rpm for 8 h. The resulting suspension was centrifuged at 600 rpm (30 g) and the resulting sedimented gel was frozen (–80°C) and freeze dried. The resulting dry powder was labeled "M". A portion of the powder was also resuspended in water to give a 20% suspension.

https://doi.org/10.1007/s42860-022-00201-9 Published online by Cambridge University Press

Raw materials were chemically pure melamine, analytically pure anhydrous sodium carbonate, and RhB, all purchased from Chengdu Kelong Chemical Reagent Factory (Chengdu, China).

Catalyst Preparation

Melamine (9.0 g) was added to 1000 mL of deionized water and stirred with a magnetic stirrer at 80°C to prepare a hot melamine solution, which was then dropped into 1000 mL of the Mnt suspension using a peristaltic pump at a speed of 1.2 mL/min. The combined suspension was stirred for 12 h at 80°C in a water bath, then dried in a vacuum freeze dryer to obtain a precursor composite. To obtain the g-C_3N_4/Mnt composites, the precursor was placed in a 50 mL corundum crucible, sealed with tin foil, and calcined for 4 h at 490, 520, 550, 580, 610, or 650°C. The heating rate was 2.3°C/min. After natural cooling, the composites were labeled as CNM-T, where CNM stands for g-C_3N_4/Mnt and T is the corresponding calcination temperature.

The same steps were taken to prepare a pure g-C_3N_4 specimen at 550°C, referred to as CN-550°C.

For the comparative study, 0.1 g of M and 1.68 g of CN-550°C were mixed and ground to obtain a physically mixed composite CN+M.

Photocatalysis Experiment

A 300 W xenon lamp, purchased from Beijing China Education Au-Light Co., Ltd, was used as the visible light source within a wavelength range of 400–800 nm. The photocatalyst (50 mg) was dispersed in RhB solution (20 mg/L, 100 mL) and then stirred for 1 h in the dark on a magnetic stirrer to reach the adsorption-desorption equilibrium. After that, the light source was turned on. Aliquots (6 mL) of the RhB solution were taken every 10 min. An Evolution 300 UV-Visible spectrophotometer (Shimadzu, Kiya-cho, Nijiyanan, Japan) was used to test the absorbance of the supernatant at the maximum absorption wavelength of RhB (554 nm), and the degradation rate of RhB was calculated according to the Beer-Lambert law (Swinehart, 1962) as follows:

$$A = log(1/T) = Kbc \quad (1)$$

$$D = (A_0 - A_t)/A_0 = (C_0 - C_t)/C_0 \quad (2)$$

where A is the absorbance; T is the transmittance; K is the molar absorption coefficient; b is the thickness of the absorbing layer; c is the concentration of the light-absorbing substance (mol/L); A_0 is the absorbance of the solution in the dark at adsorption equilibrium; A_t is the absorbance of the solution at time t of light radiation; C_0 is the solution concentration in the dark at adsorption equilibrium (mg/L); and C_t is the solution concentration at time t of the photocatalytic reaction (mg/L).

Characterization

Thermal performance analysis of samples was conducted in ambient atmospheric air using a STA449F5 synchronous thermal analyzer (TG-DSC) (NETZSCH, Berlin, Germany). Specimens were heated within a temperature range of 35–800°C at a heating rate of 20°C/min, and α-Al_2O_3 powder was taken as the reference material.

X-ray diffraction (XRD) patterns of samples were collected within a scanning angular range of 3 to 80°2θ by an Ultima IV X-ray diffractometer (PANalytical B.V., Eindhoven, The Netherlands) with a CuKα radiation source operating at a voltage of 40 kV and a tube current of 40 mA. The XRD patterns were analyzed using *Jade 6.0* software (Huang & Li, 2012).

The micromorphology of specimens was probed by means of an Ultra 55 field emission scanning electron microscope (Carl ZeissNTS GmbH, Oberkochen, Germany) with a MnKα radiation source, operating at a voltage of 15 kV and an energy resolution >127 eV. The optical images were recorded at a count rate of 20,000 cps.

The specific surface areas of samples were determined using an Autosorb-1MP aperture analyzer (American Kangta Instruments Co., Ltd, Florida, USA). The experiments were made at a degassing temperature of 200°C for 6 h.

The optical properties were analyzed using a Shimadzu UV-3700 solid ultraviolet-visible-near-infrared spectrophotometer (Shimadzu, Kiya-cho, Nijiyanan, Japan) within the scanning range 200–800 nm at a resolution of 0.1 nm. $BaSO_4$ was employed as a reference sample.

The spectroscopic analysis was performed on powder specimens using a Frontier Fourier-transform Mid/Far Infrared spectrometer (PerkinElmer, Waltham, Massachusetts, USA). The data were collected over the range 4000–400 cm^{-1}.

https://doi.org/10.1007/s42860-022-00201-9 Published online by Cambridge University Press

The absorbance of RhB solution was analyzed by an Evolution 300 UV spectrophotometer (Shimadzu, Kiyacho, Nijiyanan, Japan) using a CEL-HXF300F3 xenon lamp as the visible light source (300 W, 400–800 nm), purchased from Beijing China Education Au-Light Co., Ltd.

Results and Discussion

Thermal Performance

The differential thermal analysis curves of the M, CN-550°C, and CNM-550°C samples (Fig. 1) revealed an exothermic peak at 118°C associated with the evaporation exotherm of adsorbed water and exchangeable cation coordination water molecules on the surface and between the layers of Mnt (Ralph & Richards, 1942) The mass loss rate of M from 25 to 180°C was 13.6%. A similar result was obtained from the exothermic peak at 112°C in the DTA curve, caused by the removal of physisorbed water of Mnt in Ref. (Shmuel et al., 1989).

The mass loss of CN-550°C from 25 to 600°C was 5.3%, which was due to the evaporation of water adsorbed on the surface and the release of volatile substances (Chang et al., 2013). This could indicate that the structure of g-C_3N_4 underwent no noticeable changes up to 600°C. However, the emergence of the exothermic peak at 735°C in the DTA curve was a testimony to the decomposition of g-C_3N_4 into NH_3 and CO_2 gases (Yan et al., 2009), thus meaning the deterioration of the g-C_3N_4 quality at temperatures above 600°C. Moreover, almost no loss occurred between 750 and 800°C, which could indicate the complete decomposition of g-C_3N_4 into gases had already occurred.

The mass loss of CNM-550°C from 25 to 600°C was 7%, greater than that of pure g-C_3N_4. The appropriate peak was associated with the evaporation of adsorbed water and the dehydroxylation reaction of Mnt in the composite. Meanwhile, unlike the CN-550°C sample, a further increase in the temperature to 750°C did not impact the quality of CNM-550°C because of the significantly improved CN thermal stability after compounding with M.

Phase Analysis

The XRD patterns of a series of samples at various calcination temperatures are shown in Fig. 2. Almost all the specimens, except that labeled as M, revealed the presence of (100) and (002) reflections at 12.97 and 27.53°2θ, respectively, which were associated with a g-C_3N_4 phase (Shi et al. 2013). No diffraction peaks of melamine were observed, meaning that the latter was decomposed and converted into g-C_3N_4. At 490°C, the full-width at half maximum (FWHM) of the (002) peak was larger and the peak intensity was weaker, indicating a decrease in the crystallinity of g-C_3N_4. With a further

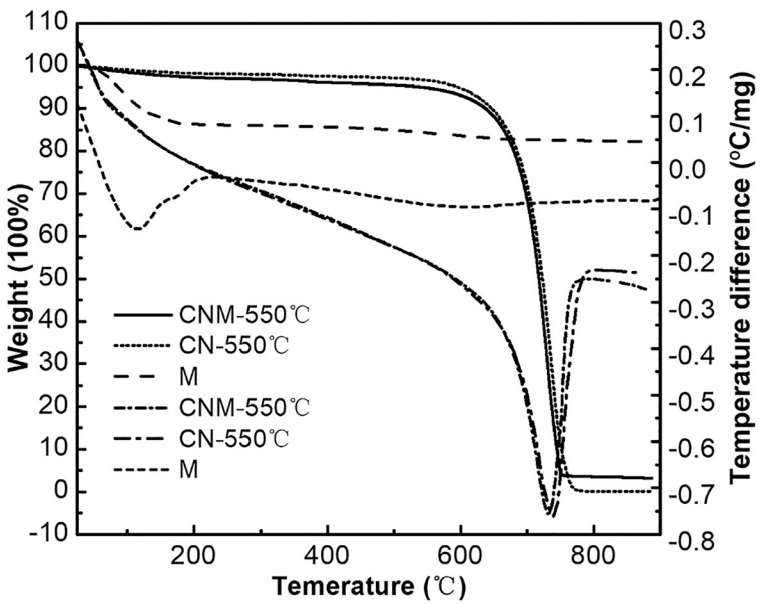

Fig. 1 Thermal curves of M, g-C_3N_4, and CNM-550°C

https://doi.org/10.1007/s42860-022-00201-9 Published online by Cambridge University Press

increase in the calcination temperature, the FWHM of (100) and (002) XRD peaks of g-C_3N_4 gradually decreased at rising peak intensities, suggesting the improvement in crystallinity of g-C_3N_4 with increasing calcination temperature. On the other hand, a lack of peaks from Mnt indicated that Mnt was stripped and dispersed in g-C_3N_4 without forming a periodic structure (Zhao & Tan, 2018). This meant that the g-C_3N_4/Mnt nanolayer composite had been prepared successfully.

Infrared Spectroscopy Data

The FTIR spectroscopic data in Fig. 3 reflected the chemical structure of the CNM-T samples. The peaks at 1640, 1569, 1326, 1412, and 1240 cm^{-1} corresponded to the tensile vibration modes of C=N and C-N heterocycles (Li, Y., et al., 2014). Their intensities increased gradually with rising temperature, indicating the increase in the degree of crystallinity of g-C_3N_4. The broad band in the range 3000–3400 cm^{-1} was due to the N–H stretching vibration and the adsorption of H_2O molecules (Li, C. et al., 2016). A strong absorption peak at 805 cm^{-1} represented the out-of-plane bending vibration of the triazine ring (Liu et al., 2015).

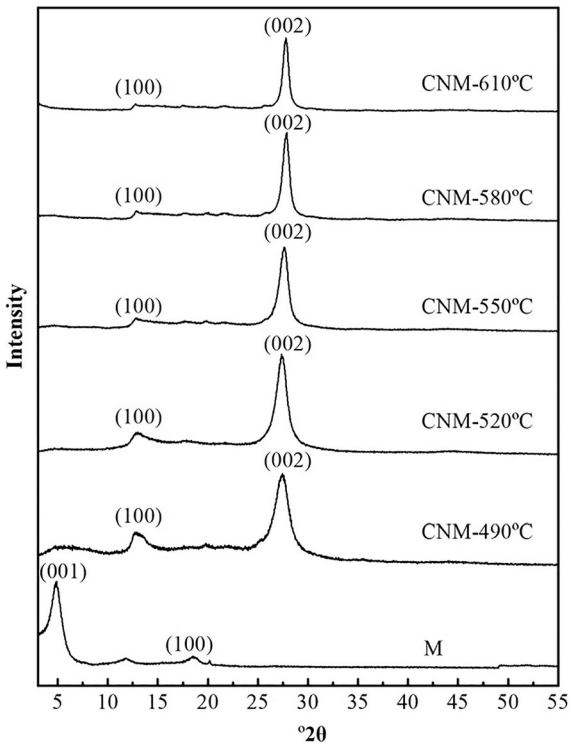

Fig. 2 XRD patterns of g-C_3N_4/Mnt composites at various calcination temperatures

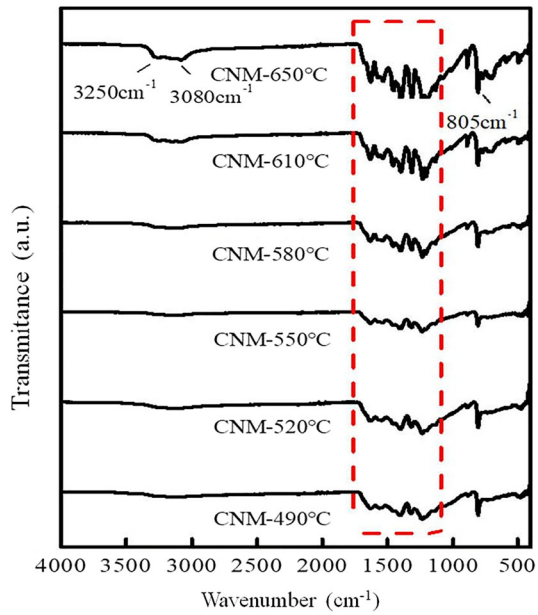

Fig. 3 FTIR spectra of g-C_3N_4/Mnt composites at various calcination temperatures

Surface Topography

Scanning electron microscopy images of Mnt nanolayers, g-C_3N_4, and g-C_3N_4/Mnt composites at different calcination temperatures (Fig. 4) revealed that the Mnt was completely exfoliated into flakes with a thickness of 5–10 nm and their diameters were 2–5 um. (Fig. 4a). The thinner the flakes, the larger the specific surface area and the surface energy, causing the flakes to wrinkle and bulge. In turn, the adsorption performance of pollutants was also enhanced. However, a block structure of the pure g-C_3N_4, caused by the large surface energy, led to the formation of pure g-C_3N_4 agglomerates. Moreover, this was not conducive to the absorption of light, resulting in the poor photocatalytic performance of g-C_3N_4.

The Mnt nanolayers were covered evenly and densely by g-C_3N_4. (Fig. 4c-h). The CN-490 sample exhibited a multi-layered stacked structure with relatively loose interlayers. According to the XRD data, this was due to the low crystallinity of g-C_3N_4 at 490°C. Furthermore, the sample surface possessed a fine granular structure owing to the impurities that remained unconverted into g-C_3N_4.

https://doi.org/10.1007/s42860-022-00201-9 Published online by Cambridge University Press

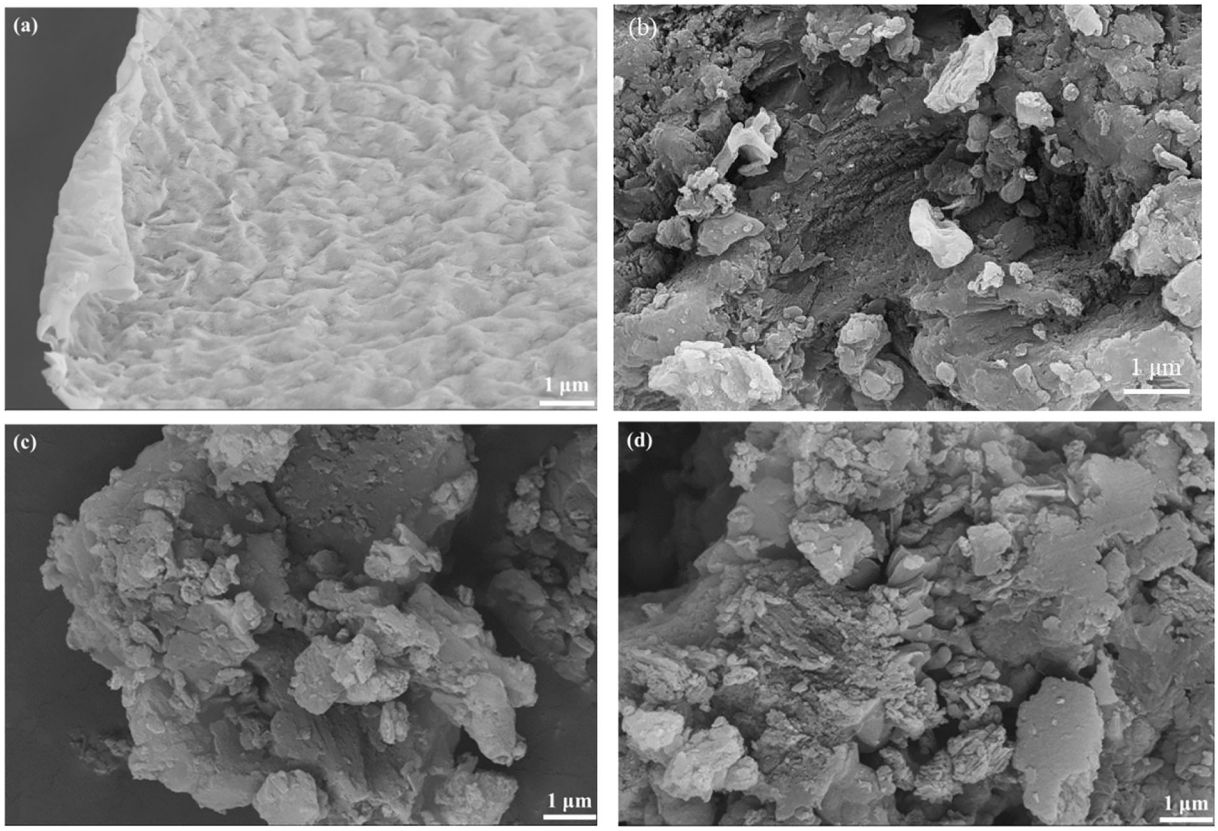

Fig. 4 SEM images of Mnt nano-particles, g-C_3N_4, and g-C_3N_4/Mnt composites at various calcination temperatures: **a** M, **b** g-C_3N_4, **c** CNM-490°C, **d** CNM-520°C, **e** CNM-550°C, **f** CNM-580°C, **g** CNM-610°C, and **h** CNM-650°C

As the calcination temperature increased from 520 to 550°C, the layered structure of the composite became clear, dense, and smooth, indicating that the crystallinity of g-C_3N_4 increased. However, the compact stacking of the lamellae led to a block structure of g-C_3N_4, thereby reducing the specific surface area and hindering the light absorption and the photocatalytic effect. At 580°C, the laminate structure of g-C_3N_4 became loose due to the fact that the heat generated by the high-temperature calcination destroyed the interlayer van der Waals forces between the g-C_3N_4 particles. As a result, the layers were separated from each other and the spacing between them increased, thereby leading to the enlargement of the specific surface area. An increase in the calcination temperature to 610°C caused a further composite peel off and the emergence of large voids on the sample surface, further increasing the specific surface area. At 650°C, the composite material exhibited a fluffy layered structure, in which flakes were peeled off into the 1–5-nm-thick layers. Moreover, the excessively high temperature caused distortion of the triazine rings in g-C_3N_4, which would affect the photocatalytic performance of CNM-650.

Specific Surface Area

The specific surface areas and the pore volumes of CNM-T, M, and CN-550°C specimens (Table 1) showed that these values increased gradually with increasing temperature. For example, the specific surface area and pore volume of CN-550°C were 5.61 m^2/g and 0.008 cm^3/g and those of CNM-550°C were 13.24 m^2/g and 0.113 cm^3/g, respectively. The maximum specific surface area and pore volume of CNM-610°C were 29.10 m^2/g and 0.251 cm^3/g, respectively. Therefore, more adsorption sites could be provided for pollutants, thereby increasing the reaction rates (Wang et al., 2018).

https://doi.org/10.1007/s42860-022-00201-9 Published online by Cambridge University Press

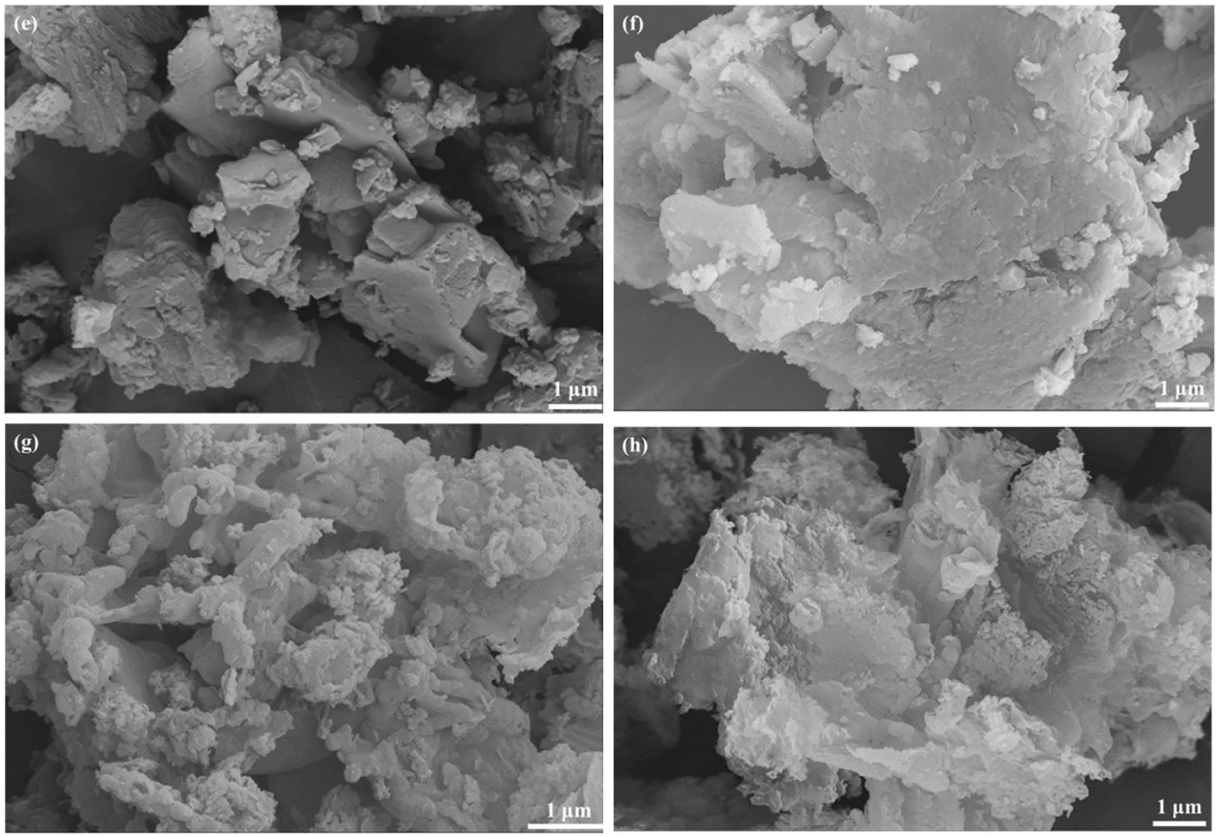

Fig. 4 (continued)

Optical Absorption Performance

The UV-Vis diffuse reflectance spectra (DRS) and the Kubelka-Munk function curves of CNM-t composites at various temperatures (Fig. 5) exhibited pronounced absorption within the visible range of 460–530 nm, which was interpreted as the electronic transition in the g-C_3N_4 semiconductor (Shi et al., 2016). Furthermore, the light absorption edge of samples gradually redshifted (to higher wavelength) with rising calcination temperature from 484 nm for CNM-490°C to 523 nm for CNM-610°C, which was due to increased pore size of specimens. This could be explained in terms of multiple reflections induced by the coarse-pore structure under light irradiation, thus allowing the catalyst to absorb more light energy and, respectively, to generate more electron-hole pairs (Liang, 2015).

In order to study further the optical properties of the composite materials, their band gap values (E_g) were calculated according to the Tauc approach (Tauc, 1974) and the Davis-Mott model (Davis & Mott, 1970) as follows:

Table 1 Specific surface areas of g-C_3N_4/Mnt composites at various calcination temperatures and of pure Mnt

Sample	M	CN-550°C	CN/M-490°C	CN/M-550°C	CN/M-610°C	CN/M-650°C
Specific surface area(m^2/g)	48.68	5.61	7.21	13.24	29.10	23.25
Pore volume (cm^3/g)	0.095	0.008	0.062	0.113	0.251	0.035

https://doi.org/10.1007/s42860-022-00201-9 Published online by Cambridge University Press

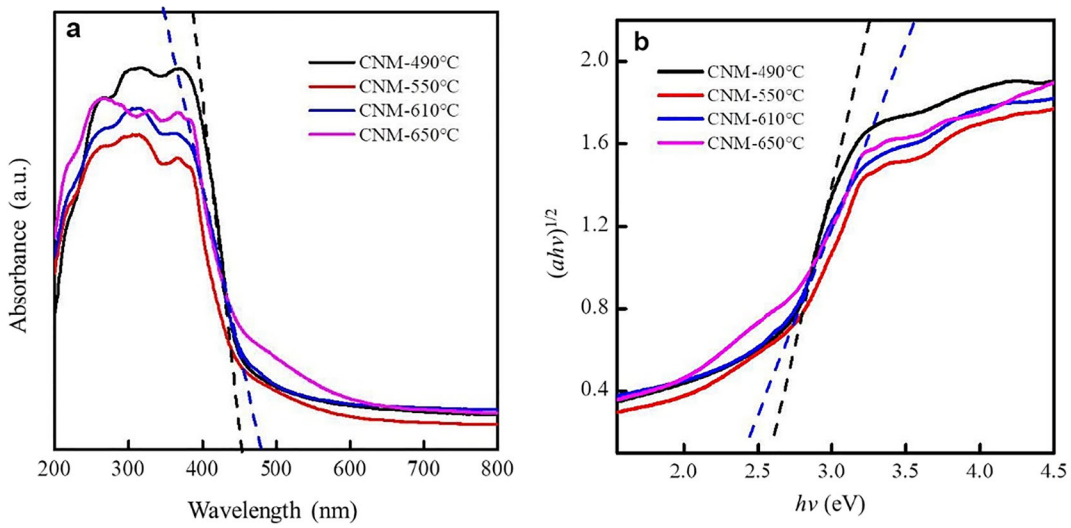

Fig. 5 **a** UV-Vis absorption spectra and **b** Kubelka-Munk function curves of CNM composites at various calcination temperatures

$$Ahv = k\left(hv - E_g\right)^{n/2} \quad (3)$$

Here, A is the adsorption coefficient; h is Planck's constant; ν is the photon frequency; and E_g represents the band gap energy; k is a constant; and n is related to the type of semiconductor.

In this respect, the band gaps of CNM-490°C, CNM-550°C, CNM-610°C, and CNM-650°C were as large as 2.56, 2.5, 2.37, and 2.4 eV, respectively, proving that the E_g of CNM-t could be reduced effectively by increasing the calcination temperature.

Photocatalytic Performance

The photocatalytic degradation rates evaluated for CN-550°C, CN+MC, and CNM-550°C (Fig. 6) showed that the self-degradation rate of RhB solution, assessed through a blank experiment under visible light irradiation, was only 6.7%, indicating the light irradiation stability of RhB. After the dark reaction for 1 h, the absorption rate of the pure g-C_3N_4 was only 1%, but increased as soon as g-C_3N_4 was compounded with Mnt nanolayers. This was because of the electrostatic attraction that made the negatively charged Mnt adsorb a large number of positively charged RhB molecules (Al-Ghouti et al., 2009). In turn, the degradation rate of CNM-550°C (97.8%) was higher than that of CN-550°C (81.5%) and CN+M (76.2%). This meant that the photocatalytic performance of composites was improved due to the loading of Mnt, causing the interaction between the g-C_3N_4 interface and the Mnt (Li, J. et al., 2016).

The photocatalytic degradation rate of CNM-490°C after a 2-h exposure to visible light irradiation was only 65% (Fig. 7). Such a low value was due to the poor crystallinity of g-C_3N_4. The best photocatalytic activity was found for CNM-610°C, the degradation rate of which also reached >95% after 60 min of visible light irradiation. The improvement of photocatalytic efficiency within the temperature range of 490 to 610°C seemed

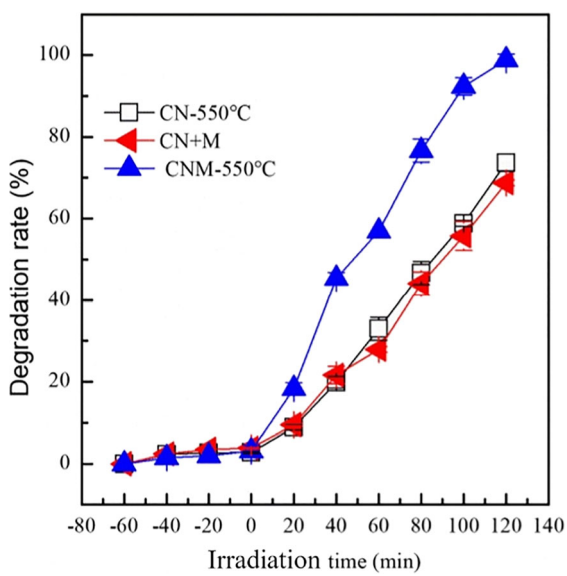

Fig. 6 Photocatalytic degradation rate of CN-550°C, CN+M, and CNM-550°C samples as a function of irradiation time

https://doi.org/10.1007/s42860-022-00201-9 Published online by Cambridge University Press

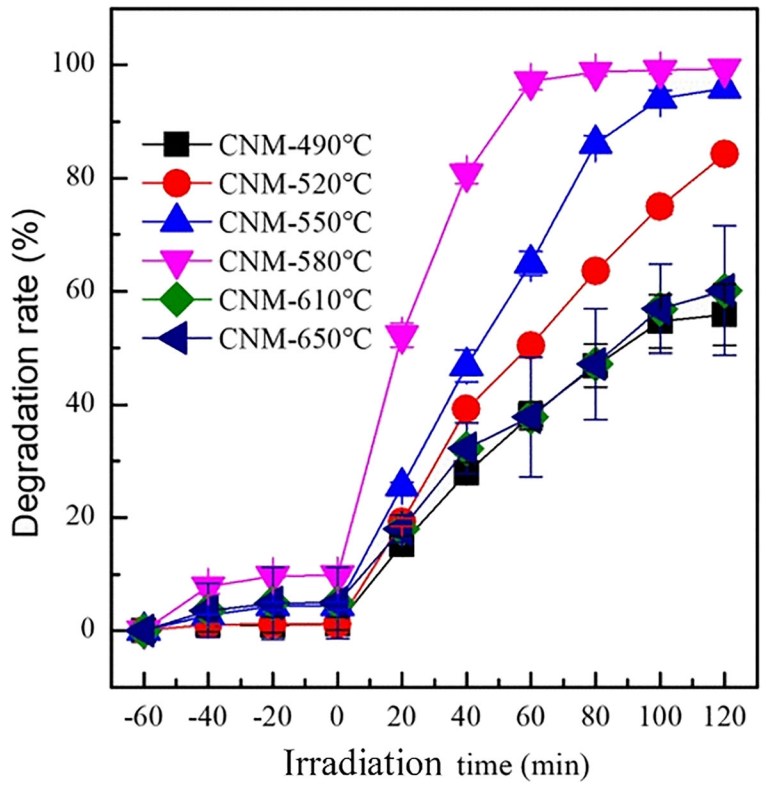

Fig. 7 Photocatalytic degradation of RhB by g-C_3N_4/Mnt composites at various calcination temperatures

to be on account of a gradual increase in the crystallinity of the composite along with a small band gap of g-C_3N_4. The changes in both the crystallinity degree and the band gap width arose from a porous sheet structure of g-C_3N_4 with a loose surface after thermal peeling. The degradation rate of the composites under higher calcination temperatures, however, underwent a sharp drop, achieving a value of 68.2% only for the CNM-650°C sample. This could be explained by the onset of decomposition of g-C_3N_4 above a threshold temperature, where a partial collapse of g-C_3N_4 nanolayers resulted in a rapid decrease in the specific surface area and pore volume, thus reducing the degradation rate and photocatalytic performance. The excellent photocatalytic effect of the composite could be attributed to two phenomena. First, the introduction of Mnt layers improved the adsorption capacity of the composite material in relation to target pollutants, promoting the interplay of g-C_3N_4 with pollutants and thereby improving the degradation efficiency of the whole composite (Li et al., 2017). Second, close contact between g-C_3N_4 and Mnt could be achieved, inducing a positive synergistic effect. As a result, the electrons generated by light excitation of g-C_3N_4 formed an electrostatic attraction between the negatively charged Mnt and the positively charged RhB molecules, which further promoted the electron exchange reaction.

Summary and Conclusions

A series of g-C_3N_4/Mnt nanolayers was prepared at various calcination temperatures, using melamine as the precursor and Mnt nanolayers as the matrix. The Mnt nanolayers in the composites were as thin as 5–10 nm and their diameters were 2–5 um. Their surface was uniformly and densely coated by g-C_3N_4 in a block-based manner, forming a multi-layered stacked structure.

An increase in temperature led to a gentle increase of the crystallinity of g-C_3N_4 along with a decrease in the band gap of the composite. Besides this, the light absorption edge gradually redshifted, and the multi-layered stack structure became dense. At 580°C, the interlayer van der Waals forces of g-C_3N_4 were destroyed by the thermal energy and the structure of

https://doi.org/10.1007/s42860-022-00201-9 Published online by Cambridge University Press

the composite material began to loosen until it was peeled off.

The conclusion was, therefore, that the combination of Mnt nanolayers and g-C_3N_4 was beneficial to the transfer of photogenerated electrons, increasing the photocatalytic effect and the degradation rate of RhB of the composite material at temperatures up to 610°C. A further increase in temperature led to a structural collapse and decomposition of g-C_3N_4; as a result, the specific surface area and the pore volume of CNM-650°C decreased rapidly along with a reduction in the photocatalytic performance.

Acknowledgments This work was supported by the National Natural Science Foundation of China (Grant No. 42072048, 41772036).

Funding Funding sources are as stated in the Acknowledgments.

Declarations

Conflict of interest The authors declare that they have no conflict of interest.

References

Al-Ghouti, M. A., Khraisheh, M., Ahmad, M., & Allen, S. (2009). Adsorption behaviour of methylene blue onto Jordanian diatomite: a kinetic study. *Journal of Hazardous Materials, 165*(1-3), 589–598.

Chang, F., Xie, Y., Li, C., Chen, J., Luo, J., Hu, X., et al. (2013). A facile modification of g-C_3N_4 with enhanced photocatalytic activity for degradation of methylene blue. *Applied Surface Science, 280*, 967–974.

Cheng, W., Shi, H., Pu, Z., & Yan, L. (2011). Synthesis and characterization of kaolinite/TiO_2 nano-photocatalysts. *Applied Clay Science, 53*, 646–649.

Davis, E. A., & Mott, N. F. (1970). Electrical and Transparent Properties of Amorphous Semiconductor. *Philosophical Magazine, 22*, 903–920.

Dong, G., Zhang, Y., Pan, Q., & Qiu, J. (2014). A fantastic graphitic carbon nitride (g-C_3N_4) material: Electronic structure, photocatalytic and photoelectronic properties. *Journal of Photochemistry and Photobiology C: Photochemistry Reviews, 20*, 33–50.

Fatimah, I., Wang, S., & Wulandari, D. (2011). ZnO/montmorillonite for photocatalytic and photochemical degradation of methylene blue. *Applied Clay Science, 53*, 553–560.

Fujishima, A., Zhang, X., & Tryk, D. (2008). TiO_2 photocatalysis and related surface phenomena. *Surface Science Reports, 63*, 515–582.

Herron, J. A., Kim, J., Upadhye, A. A., Huber, G. W., & Maravelias, C. T. (2015). A general framework for the assessment of solar fuel technologies. *Energy & Environmental Science, 8*, 126–157.

Huang, J., & Li, Z. (2012). *X-ray diffraction of polycrystalline materials: experimental principle, method and application [M]*. Metallurgical Industry Press.

Kumar, S., Karthikeyan, S., & Lee, A. (2018). g-C_3N_4-Based Nanomaterials for Visible Light-Driven Photocatalysis. *Catalysts, 8*(74), 1–47.

Li, C., Sun, Z., Huang, W., & Zheng, S. (2016). Facile synthesis of g-C_3N_4/montmorillonite composite with enhanced visible light photodegradation of rhodamine B and tetracycline. *Journal of the Taiwan Institute of Chemical Engineers, 66*, 363–371.

Li, C., Sun, Z., Zhang, W., Yu, C., & Zheng, S. (2018). Highly efficient g-C N /TiO /kaolinite composite with novel threedimensional structure and enhanced visible light responding ability towards ciprofloxacin and s. aureus. *Applied Catalysis B Environmental, 220*, 272–282.

Li, J., Liu, E., Ma, Y., Hu, X., Wan, J., Sun, L., & Fan, L. (2016). Synthesis of MoS_2/g-C_3N_4 nanosheets as 2D heterojunction photocatalysts with enhanced visible light activity. *Applied Surface Science, 364*(28), 694–702.

Li, P. P., Huang, L.Y., Li, Y.P., Xu, Y.G., Huang, S.Q., Yuan, D., Xu, H., & Li, H.M. (2017). Synthesis of dark orange montmorillonite/g-C N composites and their applications in the environment. *Journal of Physics & Chemistry of Solids, 107*, 131–139.

Li, S., Kun, C., Huabin, Z., Xiao, H., Liuqing, Y., Tao, W., & Jinhua, Y. (2016). Drastic Enhancement of Photocatalytic Activities over Phosphoric Acid Protonated Porous g-C_3N_4 Nanosheets under Visible Light. *Small, 12*(32), 4431–4439.

Li, Y., Zhan, J., Huang, L., Xu, H., Li, H., Zhang, R., & Wu, S. (2014). Synthesis and photocatalytic activity of a bentonite/g-C N composite. *RSC Advances, 4*(23), 11831–11839.

Liang, Q. (2015). Holey Graphitic Carbon Nitride Nanosheets with Carbon Vacancies for Highly Improved Photocatalytic Hydrogen Production. *Advanced Functional Materials, 25*(44), 6885–6892.

Liu, L., Shi, Y., Yu, B., Tai, Q., Wang, B., Feng, X., Liu, H., Wen, P., Yuan, B., & Hu, Y. (2015). Preparation of layered graphitic carbon nitride/montmorillonite nanohybrids for improving thermal stability of sodium alginate nanocomposites. *RSC Advances, 5*(16), 11761–11765.

Peng, K., Fu, L., Ouyang, J., & Yang, H. (2016). Emerging Parallel Dual 2D Composites: Natural Clay Mineral Hybridizing MoS_2 and Interfacial Structure. *Advanced Functional Materials, 26*(16), 2666–2675.

Ralph, E. G., Richards, A. R. (1942). Differential thermal analysis of clay minerals and other hydrous materials. part 1. *American Mineralogist, 27*(11), 746–761.

Shi, Y.Q., Jiang, S.H., Zhou, K.Q., Wang, B.B., Gui, G., Hu, Y., & Yuen, K.K. (2013). Facile preparation of ZnS / g-C_3N_4 nanohybrids for enhanced optical properties. *RSC Advances, 4*(6), 2609–2613.

Shi, L., Chang, K., Zhang, H., Hai, X., Yang, L., Wang, T., & Ye, J.H. (2016). Drastic Enhancement of Photocatalytic Activities over Phosphoric Acid Protonated Porous g-C N Nanosheets under Visible Light. *Small, 12*(32), 4431–4439.

Shmuel, Y., Müller-Vonmoos, M., Gunter, K., & Anton, R. (1989). Thermal analytic study of the adsorption of crystal violet by montmorillonite. *Thermochimica Acta, 148*(6), 457–466.

Sonawane, S.H., Gumfekar, S.P., Kate, K.H., Meshram, S.P., Kunte, K.J., Ramjee, L., Mahajan C.M., Parande M.G., & Ashokkumar M. (2010). Hydrodynamic cavitation-assisted synthesis of nanocalcite. *International Journal of Chemical Engineering,* 2010, 1–8.

Sun, Z., Chen, Y., Qiang, K., Ye, Y., & Yuan, J. (2002). Photocatalytic degradation of a cationic azo dye by TiO_2/bentonite nanocomposite. *Journal of Photochemistry and Photobiology, A: Chemistry, 149*, 169–174.

Swinehart, D.F. (1962). The Beer-Lambert Law. *Journal of Chemical Education*, *39*(7), 333–335.

Tauc, J. (1974). Optical Properties of Amorphous Semiconductors. *Amorphous and Liquid Semiconductors., 4*, 159–220.

Thomas, A., Fischer, A., Frederic, Goettmann, F., Antonietti, M., Muller, J.O., Schlogl, R., & Carlsson, J.M. (2008). Graphitic carbon nitride materials: variation of structure and morphology and their use as metal-free catalysts. *Journal of Materials Chemistry, 18*(41), 4893–4908.

Wang, X.C., Maeda, K., Thomas, A., Takanabe, K., Xin, G., Carlsson, J.M., Domen, K., & Antonietti, M. (2009). A metal-free polymeric photocatalyst for hydrogen production from water under visible light. *Nature Material, 8*, 76–80.

Wang Y.Y., Zhao, S., Zhang, Y.W., Chen, W.X., Yuan, S.H., Zhou, Y.M., & Huang, Z.W. (2018). Synthesis of graphitic carbon nitride with large specific surface area via copolymerizing with nucleobases for photocatalytic hydrogen generation. *Applied Surface Science, 463*, 1–8.

Xue, J., Ma, S., Zhou, Y., Zhang, Z., & He, M. (2015). Facile photochemical synthesis of Au/Pt/g-C_3N_4 with plasmon-enhanced photocatalytic activity for antibiotic degradation. *ACS Applied Materials & Interfaces, 7*, 9630–9637.

Yan, S. C., Li, Z. S., & Zou, Z. G. (2009). Photodegradation performance of g-C_3N_4 fabricated by directly heating melamine. *Langmuir, 25*, 10397–10401.

Zhao, W., & Tan, W. F. (2018). Quantitative and structural analysis of minerals in soil clay fractions developed under different climate zones in China by XRD with Rietveld method, and its implications for pedogenesis. *Applied Clay Science, 162*, 351–361.

https://doi.org/10.1007/s42860-022-00201-9 Published online by Cambridge University Press